

RSC Advances



This is an *Accepted Manuscript*, which has been through the Royal Society of Chemistry peer review process and has been accepted for publication.

Accepted Manuscripts are published online shortly after acceptance, before technical editing, formatting and proof reading. Using this free service, authors can make their results available to the community, in citable form, before we publish the edited article. This *Accepted Manuscript* will be replaced by the edited, formatted and paginated article as soon as this is available.

You can find more information about *Accepted Manuscripts* in the [Information for Authors](#).

Please note that technical editing may introduce minor changes to the text and/or graphics, which may alter content. The journal's standard [Terms & Conditions](#) and the [Ethical guidelines](#) still apply. In no event shall the Royal Society of Chemistry be held responsible for any errors or omissions in this *Accepted Manuscript* or any consequences arising from the use of any information it contains.

**Synthesis of ternary graphene/molybdenum oxide/poly
(p-phenylenediamine) nanocomposites for symmetric supercapacitors**

**Dan Li^a, Yurong Liu^{a,b}, Baoping Lin^{*a}, Changwei Lai^a, Ying Sun^a, Hong Yang^a,
Xueqin Zhang^a**

*(a School of Chemistry and Chemical Engineering, Southeast University, Nanjing,
Jiangsu Province 211189, China*

*b Research Institute for New Materials Technology, Chongqing University of Arts and
Science, Chongqing 402160, China*

*Corresponding author: Tel.: +86 025 52090616; fax: +86 025 52090616; E-mail
addresses: lbp@seu.edu.cn)*

Abstract: A novel ternary graphene/molybdenum oxide/poly (p-phenylenediamine) nanocomposite (GMP) has been successfully synthesized via a two-step process including the generation of binary graphene/MoO₃ composites through a hydrothermal method and the chemical polymerization of p-phenylenediamine (pPD) monomer. When the feed ratio of pPD to Na₂MoO₄·2H₂O is 1, the resulting composite(GMP-1.0) possesses superior electrochemical performance with a maximum specific capacitance of 1042.6 F g⁻¹ at 1 A g⁻¹ in a three-electrode system and 418.5 F g⁻¹ at 1 A g⁻¹ in a two-electrode system. Its energy density achieves 24.56 Wh kg⁻¹ at a power density of 325 W kg⁻¹, and 6.8 Wh kg⁻¹ at a high power density of 3263 W kg⁻¹. Furthermore, the ternary composite retains 86.7% of the initial capacitance after 3000 cycles, indicating its excellent cycling stability.

Keywords: Graphene, Molybdenum oxide, Poly (p-phenylenediamine), Ternary

composites, Supercapacitor.

1. Introduction

Nowadays, the urgent demand for new energy and sustained attention to pollution have activated intense research on novel environmentally-friendly and sustainable energy storage devices, including fuel cells, batteries, conventional capacitors and supercapacitors¹⁻³. Among them, supercapacitors are considered as the most promising candidate for energy storage due to their high power density, long cycle life, simple fabrication, low maintenance cost and rapid charging-discharging rates⁴⁻⁷. However, the relatively lower energy density compared with batteries is a major disadvantage of current supercapacitors, which can be overcome by improving specific capacitance and potential window^{8,9}. Therefore, seeking for suitable electrode materials for supercapacitors has been a significant issue.

Generally, carbon materials, conducting polymers and transition metal oxides are widely used as electrode materials for supercapacitors¹⁰⁻¹². Pseudocapacitive materials including conducting polymers and transition metal oxides are explored for preparing supercapacitors with increased capacitance and higher energy density on account of fast redox reaction¹³. In terms of transition metal oxides, ruthenium oxide (RuO_2) is considered as the best material due to its high specific capacitance¹⁴⁻¹⁶. However, its expensive production cost has brought about lots of obstacles for its practical application. Other low-cost alternatives such as MnO_2 ¹⁷⁻¹⁹, Co_3O_4 ²⁰⁻²², NiO ^{23, 24}, ZnO ^{25, 26} and MoO_3 ^{27, 28} have gradually emerged. Among these candidates, molybdenum trioxide (MoO_3) is recognized as a promising electrode material owing

to its high electrochemical activity, low cost and environmentally benign nature²⁹⁻³³. For conducting polymers, polyaniline (PANI) and its derivatives have got widespread concern due to their simple preparation, outstanding electrical conductivity and high capacitive performance^{28, 34, 35}. Poly (p-phenylenediamine) (PpPD) synthesized via in-situ polymerization of p-phenylenediamine (pPD), which contains more nitrogen atoms and active sites, is one kind of predominant derivatives of polyaniline³⁶. Since these two components possess high capacitive performance, the binary composite based on MoO₃ and PpPD are expected to possess enhanced specific capacitance. Nevertheless, the main drawbacks of this binary hybrid are poor cycling stability and rate capability because it fails to sustain fast electron transport in the case of high rates³⁷⁻³⁹.

To solve this problem, utilizing a scaffold, which possesses high surface area, to further control the structures of active materials and prevent the mechanical deformation is widely recognized as an effective method^{40, 41}. Graphene is one of the most typical carbon materials, which has attracted intensive attention for its high specific surface area, excellent electrochemical stability and good mechanical properties⁴²⁻⁴⁵. It has been verified that combining metal oxides, polymers and graphene can get novel ternary composites, which not only have enhanced specific capacitance, but also possess superior cycle stability and rate capability. Notably, a ternary cobalt ferrite/graphene/polyaniline nanocomposite⁴⁶ has been designed and fabricated by Wang et al. Its specific capacitance is up to 1133.3 F g⁻¹ at 1 mV s⁻¹, which is significantly higher than those of binary composites (The capacities of binary

cobalt ferrite/graphene, binary cobalt ferrite/ polyaniline, binary graphene/polyaniline are calculated to be 254.5 F g^{-1} , 48.3 F g^{-1} and 615.3 F g^{-1} , respectively). What's more, graphene/ Fe_2O_3 /Polyaniline, nitrogen-doped graphene/nickel ferrite/polyaniline, sulfonated graphene/ MnO_2 -/polyaniline composites possess increased capacitance of 638 F g^{-1} at 1 mVs^{-1} , 645.0 F g^{-1} at 1 mV s^{-1} and 276 F g^{-1} at 1 A g^{-1} respectively⁴⁷⁻⁴⁹. Similarly, 184 F g^{-1} for GE/ SnO_2 /PEDOT⁵⁰, 616 F g^{-1} for graphene/ SnO_2 /PPy⁵¹, 320.6 F g^{-1} at 1 mV s^{-1} for GR/ MnO_x /PPy⁵² have also been reported by researchers. Hence, according to these theoretical analysis and experimental results, it is strongly believed that ternary composites possess better electrochemical performance than binary hybrids due to the synergistic effect among three components.

In this study, the above mentioned graphene, MoO_3 and PpPD are chosen as three main components. We report a facile two-step method for the preparation of novel ternary graphene/ MoO_3 /PpPD (GMP) nanocomposite for the first time. The specific procedure is shown in Fig.1. Above all, the reduction of GO and the generation of MoO_3 nanorods occur simultaneously using a hydrothermal method, which generates binary graphene/ MoO_3 (GM) composite. Then, an in-situ polymerization of pPD is facilitated to further incorporate PpPD into binary GM composite. Here, MoO_3 and PpPD can not only provide high faradic capacitance, but also act as spacers, which can hold back the agglomeration and stacking of the graphene sheets^{53,54}. Moreover, graphene is supposed to control the size of MoO_3 and PpPD, leading to excellent cycle stability and rate capability. Furthermore, graphene and PpPD containing lots of nitrogen are able to act as a conductive network to

further increase the electrochemical activity of electrode materials. Therefore, such a ternary composite possessing superior electrochemical performance is expected to play a major role in energy storage and conversion, especially for supercapacitor applications.

2. Experimental section

2.1 Preparation of binary graphene/MoO₃ (GM) composites

GO was fabricated according to the modified Hummers method⁵⁵, and dispersed in distilled water with sonication to obtain homogeneous 1 mg/ml GO solution. The synthetic procedure of binary graphene/MoO₃ (GM) composite was as follows: 20 mL distilled water containing 0.2 g Na₂MoO₄·2H₂O and a small amount of NaCl was incorporated into 50 mL homogeneous GO solution, followed by magnetic stirring for 4 h. Then, 3 M aqueous HCl solution was added into the mixture slowly with continuous stirring to reach a pH of 2. Finally, this acid solution was transferred into a 100 mL Teflon-lined stainless steel autoclave and kept at 180°C for 24 h to obtain a binary GM composite.

2.2 Preparation of ternary graphene/MoO₃/PpPD (GMP) composites

Ternary graphene/MoO₃/PpPD (GMP-x) composites (the feed ratio of pPD to Na₂MoO₄·2H₂O was labeled as x) was synthesized through chemical polymerization of p-phenylenediamine monomers on the basis of binary GM. A typical experiment for the synthesis of ternary GMP-1.0 nanocomposite was used as an example. 0.2 g p-phenyldiamine (pPD) dissolving in 40 mL N, N-Dimethylformamide (DMF) was added into the as-prepared GM solution with continuous stirring to obtain a

homogenous solution in an ice bath. Then, the chemical polymerization of pPD was initiated by the right amount of ammonium persulfate (APS) solution with the drop-wise addition and stirred for 24 h at around 0°C. The final ternary GMP-1.0 composite was obtained by filtration, washing and drying at 70°C under vacuum overnight. The other ternary GMP hybrids (GMP-0.25, GMP-0.5, GMP-1.6, GMP-2.0, GMP-2.5) with different amount of pPD were also prepared using the same method. The binary graphene/PpPD (GP) composites were prepared via a similar procedure without the addition of Na₂MoO₄·2H₂O and NaCl and the binary MoO₃/PpPD (MP) composite was synthesized without GO added. The pure reduced graphene, MoO₃ and PpPD were also prepared for comparison.

2.3 General characterizations

X-ray diffraction (XRD) was performed on a D8 Advance (Bruker-AXS, Germany). Raman analysis was carried out using a Renishaw inVia Raman Microscope utilizing a 532 nm argon ion laser. The existence of typical functional groups was probed by FT-IR on a Nicolet 5700 spectrophotometer (Thermo Electron Scientific Instruments Corp., USA). Detailed elemental analysis was carried out using an ESCALAB-250 X-ray photoelectron spectroscopy (XPS) (Thermo Fisher Scientific, USA). The morphology analysis was performed on HITACHI S-4800 SEM, FEI Sirion SEM, FEI G2-20 and Philips Tecnai-12 TEM. BET analysis was carried out on Nova 1200e (Quantachrome, USA).

2.4 Electrochemical characterization of GMP

The working electrode was obtained by mixing the as-prepared active material,

acetylene black and polyvinylidene difluoride (PVDF) with a mass ratio of 8:1:1, followed by the addition of N-methylpyrrolidone (NMP) to form a homogenous slurry. Then, the slurry was coated on a piece of carbon paper and dried at 70 °C in a vacuum oven. The electrochemical performances were tested in a three-electrode system using platinum wires, saturated calomel electrode (SCE) and 1 M H₂SO₄ as counter electrodes, reference electrode and electrolyte, respectively. Cyclic voltammetry (CV), galvanostatic charge/discharge (GCD) and alternating current (AC) impedance tests were carried out on a CHI660E electrochemical workstation with a scan range of 0 to 1.0 V. In a two-electrode system, the symmetric GMP-1.0//GMP-1.0 supercapacitor was assembled by GMP-1.0 acting as both electrodes and a polymer separator soaked with 1 M H₂SO₄. CV and GCD tests were also performed by a CHI660E workstation with a scan range of 0 to 0.65 V.

The specific capacitance of electrode materials can be calculated according to the following formula on the basis of CV and GCD curves respectively⁵⁶⁻⁵⁸:

$$C = \frac{\int Idv}{vmV} \quad (1)$$

Where C is the specific capacitance (F g⁻¹), I is the response current (A), V is the potential drop (V), v is the scan rate (V s⁻¹) and m is the mass of the active material

(g).

$$C = \frac{I\Delta t}{mV} \quad (2)$$

Where Δt is the discharge time in s and the meaning of other parameters is the same as above.

The energy density (E, Wh kg⁻¹) and power density (P, W kg⁻¹) of the assembled supercapacitors could be evaluated according to equation 3 and 4^{46, 59}:

$$E = \frac{1}{2}CV^2 \quad (3)$$

$$P = \frac{E}{t} \quad (4)$$

Where C is the specific capacitance ($F\ g^{-1}$), V is the potential drop (V), and the discharge time (h).

3. Results and discussion

3.1 Characterization of resulting samples

Fig. 2 shows XRD patterns of the as-prepared samples. In terms of MoO_3 , the characteristic diffraction peaks centered at 12.6° , 23.3° , 25.6° , 27.3° , 33.8° and 38.9° correspond to (020) (110) (040) (021) (111) and (060) crystal planes, respectively⁶⁰. The obvious and sharp peaks of MoO_3 are all in good agreement with the standard peaks of α - MoO_3 (JCPDS card no. 05-0508), which indicates the successful formation of pure MoO_3 . For GO, its diffraction peak at the 2θ value of 10.01° assigned to (002) and the corresponding interlayer space of 0.88 nm, which is much higher than graphite, reveal that graphene oxide with lots of oxygen functional groups is formed as expected⁶¹. On the other hand, combining the spectra of GO, pure graphite (JCPDS card no. 26-1079) and GMP-1.0, the non-existence of these two peaks at 10.01° and 26.6° indicates that GO is reduced and exfoliated successfully under hydrothermal condition for GMP-1.0. However, because of the strong intensity of peaks from MoO_3 , the broad peaks with low intensity at around 26° assigned to graphene and PpPD can't be seen easily. Fortunately, compared with the spectrum of pure MoO_3 , the half-peak breadth of GMP-1.0 ranging from 20° to 30° are all bigger, which may attribute to the appearance of amorphous PpPD³⁶. Therefore, On the basis

of the above analysis, all typical peaks of MoO₃ and PpPD can be observed in the XRD spectrum of GMP-1.0 and other binary composites (Fig.S1), indicating the ternary GMP composites and corresponding binary composites have been successfully fabricated.

The Raman testing is widely known as an effective method to analyze carbon-based materials. Fig.3 presents the Raman spectra of pure components and ternary GMP-1.0. For GO and GMP-1.0, two obvious and typical peaks centered at 1356 and 1600 cm⁻¹ are indexed as D band and G band of graphene⁶². Two other peaks at 2675 and 2973 cm⁻¹ in the enlarged spectrum of GMP-1.0 can be assigned to 2D, D + G band respectively, verifying the formation of graphene strongly⁶³. Compared with the D/G ratio between GO and GMP-1.0, there is a slight increase from 0.96 for GO to 1.06 for GMP-1.0, which may be attributed to the formation of PpPD containing lots of small sp² domains. Furthermore, 2D band shifting from 2668 cm⁻¹ in GO to 2675 cm⁻¹ in GMP-1.0 suggests a slight increase of layers for graphene, indicating that MoO₃ and PpPD can prevent serious aggregation of graphene sheets. In addition, according to the comparison of BET analysis between binary MP and ternary GMP-1.0 in Fig.S2, the point that graphene nanosheets can conversely prevent the agglomeration of the binary MoO₃/PpPD composite materials can also be revealed easily. On the other hand, for PpPD, the broad peaks at around 525 and 2774 cm⁻¹ can be ascribed to out of plane C–N–C torsion and N-H stretching vibration. And other obvious peaks centered at 1182, 1346, 1405, 1520 and 1602 cm⁻¹ are assigned to in plane C–H bending, C–N⁺ stretching modes, C–N, C–C and C=N of quinonoid ring

respectively, which are mixed with the two typical bands of graphene and hardly distinguished in the Raman spectrum of GMP-1.0⁶⁴. In terms of MoO₃, there are a lot of peaks corresponding to various bending modes of α -MoO₃. Characteristic peaks of pure MoO₃ at 159 cm⁻¹ (translational rigid MoO₄ chain mode), 291 cm⁻¹ (wagging vibrations of O-Mo-O), 335 cm⁻¹ (bending vibration of O-Mo-O), 668 cm⁻¹ (asymmetrical stretching vibration of O-Mo-O), 817 cm⁻¹ (symmetrical stretching vibrations of Mo=O) and 993 cm⁻¹ (asymmetrical stretching vibrations of Mo=O bonds) can also be seen in the spectrum of GMP-1.0, which reveals the successful incorporation of MoO₃⁶⁵. Combing Fig. 3 and Fig.S3, the successful preparation of binary composites and ternary GMP can also be revealed easily.

Further, in order to indicate the existence of a variety of functional groups of three components, the FT-IR spectra of as-prepared materials are shown in Fig. 4. For GO, four typical peaks at 3420, 1735, 1618 and 1095 cm⁻¹ corresponding to -OH, C=O in -COOH, C=C, C-O in epoxy functional groups respectively, which can substantiate the successful preparation of GO⁶⁶. Furthermore, the characteristic peaks of MoO₃ at 995, 873 and 552 cm⁻¹ attributed to terminal Mo=O, the stretching vibration of Mo-O-Mo and bending vibration of Mo-O-Mo, which also can be found in the spectrum of GMP-1.0, corroborate the incorporation of MoO₃ in ternary composites⁶⁵. On the other hand, obvious peaks at around 3155 cm⁻¹ (stretching vibration of N-H), 1567 cm⁻¹ (stretching vibration of C=C), 1503 cm⁻¹ (stretching vibration of C=N), 1288 cm⁻¹ (C-N), 1106 cm⁻¹ (plane bending vibration of C-H) and 821 cm⁻¹ (out-of-plane bending vibration of C-H) of PpPD appearing in GMP-1.0

have significant blue-shift phenomenon, attributed to the strong interactions between graphene and PpPD backbone, which also verify the addition of PpPD in ternary composites^{36, 65, 67}.

The composition of as-prepared samples can be further analyzed by XPS measurement (Fig.5). The wide scan XPS spectrum of ternary GMP-1.0 suggests that it contains four main components(C, O, N, Mo) and the weight percentage of Mo is 8.76%. After easy calculation, the weight percentage of MoO₃ is 13.1% in the ternary composite. Fig. 5(b) shows two symmetrical peaks at 236 and 232.9 eV with 3.1 eV peak-to-peak separation, which are in good agreement with standard data of MoO₃, while N 1s XPS core spectrum (Fig. 5(c)) on the basis of 80% Gaussian and 20% Lorentzian shape can be deconvoluted into three typical peaks at 401.0, 398.9 and 397.0 eV assigned to -NH*, -NH- and -N= respectively , which are consistent with the main chemical states of N in PpPD^{68, 69}. The successful fabrication of ternary GMP can also be revealed by the XPS C 1s core-level spectra in Fig. 5(d) and (e). The C 1s spectrum of GO is deconvoluted into four peaks at 284.8, 286.8, 287.6 and 288.5 eV, which correspond to C-C, C-O, C=O and O-C=O⁷⁰. In terms of GMP-1.0, the existence of these four typical peaks with a slight shift and appearance of a new peak at 285.4 eV indexed as C-N reveal that PpPD is formed as expected⁵⁷. What's more, the intensities of some oxygenated functional groups suffer from a significant decrease, which implies the successful reduction of GO under hydrothermal condition. Hence, according to the wide scan spectra and the comparison of C 1s and O 1s spectra (Fig.S4) between GO and ternary GMP-1.0 composite, resulting composites

can be indicated obviously.

Fig.6 (a) - (e) shows the morphology of ternary GMP-1.0 and pure components. On the basis of the comparison between GO and ternary GMP-1.0, the co-existence of three components in ternary GMP-1.0 can be revealed easily, while MoO₃ nanorods and PpPD nanoparticles are tightly coated on the graphene sheets with the layered structure and wrinkle. On the other hand, according to the SEM images of Fig.6(c)-(d), MoO₃ nanorods with an average diameter of around 200 nm and PpPD nanoparticles can be seen obviously. Due to a large amount of MoO₃ and PpPD and a tiny quantity of graphene added into ternary composites, layered graphene nanosheets can't be observed directly in the SEM image of ternary GMP-1.0 in Fig.6 (e). However, for the ternary GMP-1.0 composite, the homogeneous distribution of different elements can be tested by elemental mappings in Fig.S5.

3.2 Electrochemical characterization

To study the electrochemical performance of as-prepared materials for electrodes, cyclic voltammetry (CV), galvanostatic charge/discharge (GCD) and alternating current (AC) impedance measurements are essential. The CV curves carried out in a three-electrode system of pure reduced graphene, MoO₃ and PpPD are recorded in Fig. 7(a). In terms of graphene, its nearly rectangular shape without obvious redox peaks reveals the character of electric-double-layer (EDL). On the other hand, a visible pair of redox peak in the CV curve of PpPD corresponding to the pseudocapacitance behavior is assigned to the invertible conversion between a semiconducting state and a conducting state, while MoO₃ also shows an obvious pair of redox peaks (0.5 to 0.6

V) corresponding to the redox reaction of MoO_3 . Fig. 7(b) shows the CV curves of binary products and ternary GMP-1.0, which have typical pairs of peaks in consistent with pure samples. There is no doubt that the area of closed CV loop and the specific capacitance of ternary GMP-1.0 is the highest, which indicates its excellent capacitive performance. On the basis of the formula (1), the specific capacitance of graphene, MoO_3 , PpPD, binary GP, binary GM, binary MP and ternary GMP-1.0 at 5 mV s^{-1} are 303.2 F g^{-1} (graphene), 1303.2 F g^{-1} (MoO_3), 346.5 F g^{-1} (PpPD), 371.2 F g^{-1} (GP), 903 F g^{-1} (GM), 1193.2 F g^{-1} (MP) and 2286.6 F g^{-1} (GMP-1.0), respectively. CV curves of ternary GMP-1.0 at different scan rates are recorded in Fig.7 (c). Notably, all the curves keep similar with the increase of scan rates, which reveals an excellent rate capability. Here, the influence of different feed ratio in ternary composites on the electrochemical performances is studied and the result is recorded in Fig.S6, which also reveals GMP-1.0 possesses the highest specific capacitance and good capacitive stability due to the reasonable feed ratio and synergistic effect.

The electrochemical performance of electrode materials is also indicated by GCD test. In Fig. 8(a)-(b) and Fig.S7 (a), the discharge time of ternary GMP-1.0 is much longer than those of other binary composites at different current densities and the curves keep a similar shape with increasing current density, which shows the high capacitance and superior rate capability of ternary GMP composites. Furthermore, the GC testing of other ternary GMP composites with differing feed ratio at 1 A g^{-1} is also performed (Fig. S7 (b)-(c)). On the basis of equation (2), the corresponding specific capacitance of these ternary hybrids is evaluated and the result that ternary GMP-1.0

possesses the highest specific capacitance (1042.6 Fg^{-1} at 1 A g^{-1}) among these ternary GMP samples can be gotten easily, which is all coincidence with the CV results.

Fig.8 (c) depicts the Nyquist plots of four composites. It is notable that ternary GMP-1.0 shows the smallest semicircle at high frequency region corresponding to the lowest internal resistance of interface and the straight line closest to 90° assigned to the best capacitive behavior. Cycle life is another standard to reveal the electrochemical performance of electrode materials. Here, ternary GMP-1.0 is subject to 3000 cycles at 12 A g^{-1} and the periodical capacitances are recorded in Fig.8 (d). Notably, GMP-1.0 retains 86.7% of initial capacitance, which shows its superior cycle stability and capacity reversibility.

3.3 Electrochemical performance of symmetric devices

The above analysis on the three-electrode system reveals that ternary GMP-1.0 possessing high specific capacitance, excellent rate capability, low resistance and superior capacitive performance is a promising candidate of electrode material for supercapacitors. Here, a symmetric supercapacitor by using ternary GMP-1.0 as both electrode materials is assembled. To further explore the electrochemical performance, the CV, GCD measurements based on the two-electrode system are carried out. Fig.9 (a) shows the CV curves at differing scan rates. It is noted that the potential window decrease to 0.65V, which may be attributed to a relatively smaller current density compared with the three-electrode system. According the CV curves, the specific capacitance at 5 mV s^{-1} is calculated to 737.7 F g^{-1} and the excellent capacitance behavior can be revealed obviously.

The GCD curves in a two-electrode system are also recorded in Fig. 9(b). Their similar asymmetric triangular shapes reveal the appearance of two energy storage mechanisms and its good rate capability. The specific capacitance of ternary GMP-1.0 is decreased from 418.5 F g^{-1} to 115.84 F g^{-1} when the current density increases from 1 to 10 A g^{-1} . According to the equation (3) and (4), the energy density and power density can be evaluated at different current densities respectively, which are shown in Fig. 9(c). The GMP-1.0// GMP-1.0 device shows a high energy density of 24.56 Wh kg^{-1} at a power density of 325 W kg^{-1} , and the energy density remains 6.8 Wh kg^{-1} at a high power density of 3263 W kg^{-1} .

The ternary GMP-1.0 composite, which possesses high specific capacitance, excellent rate capability and cycle stability, low resistance and relatively high energy density, could attribute to the synergistic effect among the three main components. First of all, MoO_3 and PpPD can provide high pseudocapacitance to enhance the whole specific capacitance and energy density of composites. Second, MoO_3 and PpPD can prevent the serious agglomeration and stacking of graphene to achieve more electric-double-layer capacitance. Besides, graphene may play a role in increasing the electrical conductivity, which is beneficial to the optimization of electrode/electrolyte contact. Furthermore, the strong interaction between graphene and PpPD with lots of N atoms, which can provide more active sites, is conducive to enhance the whole electrochemical activity remarkably. In addition, graphene nanosheets are added to control the structure and size of MoO_3 and PpPD, leading to excellent electrochemical stability. Therefore, the ternary GMP-1.0 composite with

reasonable feed ratio has better electrochemical performance than pure components, all binary composite and other ternary composites with unsuitable contents.

4. Conclusion

In summary, a ternary graphene/molybdenum oxide/poly (p-phenylenediamine) nanocomposite is fabricated via a two-step method and the influence of feed ratio on electrochemical performances is also explored. It is found that the ternary GMP-1.0 composite possesses the best electrochemical performance among pure components, corresponding binary composites and other ternary composites due to the synergistic effects. Here, MoO₃ and PpPD can provide higher pseudocapacitance and energy densities, while graphene sheets acting as a support is able to enhance the electrical conductivity and electrochemical stability. The specific capacitance of ternary GMP-1.0 is up to 1042.6 F g⁻¹ at 1 A g⁻¹ in a three-electrode system and 418.5 F g⁻¹ at 1 A g⁻¹ using a two-electrode system, while the high energy density reaches 24.56 Wh kg⁻¹ at a power density of 325 W kg⁻¹, and 6.8 Wh·kg⁻¹ at a high power density of 3263 W kg⁻¹. Furthermore, a negligible decay of only 13.3% of the initial capacitance after 3000 cycles reveals the excellent cycle stability. Therefore, the resulting ternary GMP-1.0 composite is considered as a promising hybrid electrode materials in the field of energy storage and conversion.

Acknowledgement

The study was supported by National Natural Science Foundation of China (No. 21304018, No. 21374016) and Jiangsu Provincial Natural Science Foundation of China (No. BK20130619).

Reference:

1. A. S. Arico, P. Bruce, B. Scrosati, J. M. Tarascon and W. Van Schalkwijk, *Nature Materials*, 2005, 4, 366-377.
2. M. Winter and R. J. Brodd, *Chemical Reviews*, 2004, 104, 4245-4269.
3. V. L. Pushparaj, M. M. Shaijumon, A. Kumar, S. Murugesan, L. Ci, R. Vajtai, R. J. Linhardt, O. Nalamasu and P. M. Ajayan, *Proceedings of the National Academy of Sciences of the United States of America*, 2007, 104, 13574-13577.
4. Y. Z. Zhang, Y. Wang, T. Cheng, W. Y. Lai, H. Pang and W. Huang, *Chemical Society reviews*, 2015, 44, 5181-5199.
5. P. H. Yang and W. J. Mai, *Nano Energy*, 2014, 8, 274-290.
6. J. Yan, Q. Wang, T. Wei and Z. J. Fan, *Advanced Energy Materials*, 2014, 4.
7. V. V. N. Obreja, *Review on Electrochemical Storage Materials and Technology*, 2014, 1597, 98-120.
8. P. J. Hall, M. Mirzaeian, S. I. Fletcher, F. B. Sillars, A. J. R. Rennie, G. O. Shitta-Bey, G. Wilson, A. Cruden and R. Carter, *Energy & Environmental Science*, 2010, 3, 1238-1251.
9. I. S. Ike, I. Sigalas, S. Iyuke and K. I. Ozoemena, *Journal of Power Sources*, 2015, 273, 264-277.
10. P. Simon and Y. Gogotsi, *Nature Materials*, 2008, 7, 845-854.
11. G. P. Wang, L. Zhang and J. J. Zhang, *Chemical Society reviews*, 2012, 41, 797-828.
12. C. Liu, F. Li, L. P. Ma and H. M. Cheng, *Advanced materials*, 2010, 22, E28-+.
13. B. E. Conway, V. Birss and J. Wojtowicz, *Journal of Power Sources*, 1997, 66, 1-14.
14. Z. S. Wu, D. W. Wang, W. Ren, J. Zhao, G. Zhou, F. Li and H. M. Cheng, *Advanced Functional Materials*, 2010, 20, 3595-3602.
15. C. C. Hu, W. C. Chen and K. H. Chang, *Journal of the Electrochemical Society*, 2004, 151, A281-A290.
16. C. C. Hu, K. H. Chang, M. C. Lin and Y. T. Wu, *Nano letters*, 2006, 6, 2690-2695.
17. W. F. Wei, X. W. Cui, W. X. Chen and D. G. Ivey, *Chemical Society reviews*, 2011, 40, 1697-1721.
18. M. Toupin, T. Brousse and D. Belanger, *Chemistry of Materials*, 2004, 16, 3184-3190.
19. X. Y. Lang, A. Hirata, T. Fujita and M. W. Chen, *Nature Nanotechnology*, 2011, 6, 232-236.
20. T. Zhu, J. S. Chen and X. W. Lou, *Journal of Materials Chemistry*, 2010, 20, 7015-7020.
21. J. A. Xu, L. Gao, J. Y. Cao, W. C. Wang and Z. D. Chen, *Electrochimica Acta*, 2010, 56, 732-736.
22. S. L. Xiong, C. Z. Yuan, M. F. Zhang, B. J. Xi and Y. T. Qian, *Chemistry-a European Journal*, 2009, 15, 5320-5326.
23. J. W. Lang, L. B. Kong, W. J. Wu, Y. C. Luo and L. Kang, *Chemical Communications*, 2008, DOI: 10.1039/b800264a, 4213-4215.
24. F. Cao, G. X. Pan, X. H. Xia, P. S. Tang and H. F. Chen, *Journal of Power Sources*, 2014, 264, 161-167.
25. P. H. Yang, X. Xiao, Y. Z. Li, Y. Ding, P. F. Qiang, X. H. Tan, W. J. Mai, Z. Y. Lin, W. Z. Wu, T. Q. Li, H. Y. Jin, P. Y. Liu, J. Zhou, C. P. Wong and Z. L. Wang, *ACS nano*, 2013, 7, 2617-2626.
26. C. Y. Cao, W. Guo, Z. M. Cui, W. G. Song and W. Cai, *Journal of Materials Chemistry*, 2011, 21, 3204-3209.
27. Q. Tang, L. Wang, K. Zhu, Z. Shan and X. Qin, *Materials Letters*, 2013, 100, 127-129.
28. F. R. Jiang, W. Y. Li, R. J. Zou, Q. Liu, K. B. Xu, L. An and J. Q. Hu, *Nano Energy*, 2014, 7, 72-79.
29. X. Xiao, T. P. Ding, L. Y. Yuan, Y. Q. Shen, Q. Zhong, X. H. Zhang, Y. Z. Cao, B. Hu, T. Zhai, L. Gong,

- J. Chen, Y. X. Tong, J. Zhou and Z. L. Wang, *Advanced Energy Materials*, 2012, 2, 1328-1332.
30. W. Tang, L. L. Liu, Y. S. Zhu, H. Sun, Y. P. Wu and K. Zhu, *Energy & Environmental Science*, 2012, 5, 6909-6913.
31. W. Tang, L. L. Liu, S. Tian, L. Li, Y. B. Yue, Y. P. Wu and K. Zhu, *Chemical Communications*, 2011, 47, 10058-10060.
32. J. Chang, M. Jin, F. Yao, T. H. Kim, V. T. Le, H. Yue, F. Gunes, B. Li, A. Ghosh, S. Xie and Y. H. Lee, *Advanced Functional Materials*, 2013, 23, 5074-5083.
33. T. Brezesinski, J. Wang, S. H. Tolbert and B. Dunn, *Nature Materials*, 2010, 9, 146-151.
34. R. Ramya, R. Sivasubramanian and M. V. Sangaranarayanan, *Electrochimica Acta*, 2013, 101, 109-129.
35. K. Wang, J. Y. Huang and Z. X. Wei, *Journal of Physical Chemistry C*, 2010, 114, 8062-8067.
36. Jaidev and S. Ramaprabhu, *Journal of Materials Chemistry*, 2012, 22, 18775-18783.
37. Y. F. Zhang, L. Q. Li, H. Q. Su, W. Huang and X. C. Dong, *Journal of Materials Chemistry A*, 2015, 3, 43-59.
38. K. Wang, H. P. Wu, Y. N. Meng and Z. X. Wei, *Small*, 2014, 10, 14-31.
39. N. A. Kumar, H. J. Choi, Y. R. Shin, D. W. Chang, L. M. Dai and J. B. Baek, *ACS nano*, 2012, 6, 1715-1723.
40. L. L. Zhang and X. S. Zhao, *Chemical Society reviews*, 2009, 38, 2520-2531.
41. F. Beguin, V. Presser, A. Balducci and E. Frackowiak, *Advanced materials*, 2014, 26, 2219-2251.
42. L. L. Zhang, R. Zhou and X. S. Zhao, *Journal of Materials Chemistry*, 2010, 20, 5983-5992.
43. M. D. Stoller, S. Park, Y. Zhu, J. An and R. S. Ruoff, *Nano letters*, 2008, 8, 3498-3502.
44. M. Pumera, *Energy & Environmental Science*, 2011, 4, 668-674.
45. X. Huang, X. Y. Qi, F. Boey and H. Zhang, *Chemical Society reviews*, 2012, 41, 666-686.
46. P. Xiong, H. J. Huang and X. Wang, *Journal of Power Sources*, 2014, 245, 937-946.
47. X. F. Xia, Q. L. Hao, W. Lei, W. J. Wang, D. P. Sun and X. Wang, *Journal of Materials Chemistry*, 2012, 22, 16844-16850.
48. W. J. Wang, Q. L. Hao, W. Lei, X. F. Xia and X. Wang, *Journal of Power Sources*, 2014, 269, 250-259.
49. G. X. Wang, Q. Q. Tang, H. Bao, X. W. Li and G. C. Wang, *Journal of Power Sources*, 2013, 241, 231-238.
50. W. J. Wang, W. Lei, T. Y. Yao, X. F. Xia, W. J. Huang, Q. L. Hao and X. Wang, *Electrochimica Acta*, 2013, 108, 118-126.
51. W. J. Wang, Q. L. Hao, W. Lei, X. F. Xia and X. Wang, *Rsc Advances*, 2012, 2, 10268-10274.
52. G. Q. Han, Y. Liu, E. J. Kan, J. Tang, L. L. Zhang, H. H. Wang and W. H. Tang, *Rsc Advances*, 2014, 4, 9898-9904.
53. M. M. Sk and C. Y. Yue, *Rsc Advances*, 2014, 4, 19908-19915.
54. Y. H. Lu, Y. Huang, F. Zhang, L. Zhang, X. Yang, T. F. Zhang, K. Leng, M. J. Zhang and Y. S. Chen, *Chinese Science Bulletin*, 2014, 59, 1809-1815.
55. Y. S. Lim, Y. P. Tan, H. N. Lim, N. M. Huang, W. T. Tan, M. A. Yarmo and C. Y. Yin, *Ceramics International*, 2014, 40, 3855-3864.
56. Y. Zhao, H. Wei, M. Arowo, X. Yan, W. Wu, J. Chen, Y. Wang and Z. Guo, *Physical Chemistry Chemical Physics*, 2015, 17, 1498-1502.
57. W. Wang, Q. Hao, W. Lei, X. Xia and X. Wang, *Rsc Advances*, 2012, 2, 10268-10274.
58. H. W. Wang, Z. A. Hu, Y. Q. Chang, Y. L. Chen, H. Y. Wu, Z. Y. Zhang and Y. Y. Yang, *Journal of*

- Materials Chemistry*, 2011, 21, 10504-10511.
59. N. Padmanathan, S. Selladurai and K. M. Razeeb, *RSC Adv.*, 2015, 5, 12700-12709.
 60. X. Yang, C. Lu, J. Qin, R. Zhang, H. Tang and H. Song, *Materials Letters*, 2011, 65, 2341-2344.
 61. Y. Jin and M. Jia, *Colloids and Surfaces A: Physicochemical and Engineering Aspects*, 2015, 464, 17-25.
 62. S. Stankovich, D. A. Dikin, R. D. Piner, K. A. Kohlhaas, A. Kleinhammes, Y. Jia, Y. Wu, S. T. Nguyen and R. S. Ruoff, *Carbon*, 2007, 45, 1558-1565.
 63. A. C. Ferrari, J. C. Meyer, V. Scardaci, C. Casiraghi, M. Lazzeri, F. Mauri, S. Piscanec, D. Jiang, K. S. Novoselov, S. Roth and A. K. Geim, *Physical Review Letters*, 2006, 97, 187401.
 64. G. A. Snook, P. Kao and A. S. Best, *Journal of Power Sources*, 2011, 196, 1-12.
 65. X. F. Xia, Q. L. Hao, W. Lei, W. J. Wang, H. L. Wang and X. Wang, *Journal of Materials Chemistry*, 2012, 22, 8314-8320.
 66. Y. Jin, S. Huang, M. Zhang and M. Jia, *Synthetic Metals*, 2013, 168, 58-64.
 67. S. Liu, B. Yu and T. Zhang, *Journal of Materials Chemistry A*, 2013, 1, 13314.
 68. C.-L. Liu, Y. Wang, C. Zhang, X.-S. Li and W.-S. Dong, *Materials Chemistry and Physics*, 2014, 143, 1111-1118.
 69. Y. Lu, F. Zhang, T. Zhang, K. Leng, L. Zhang, X. Yang, Y. Ma, Y. Huang, M. Zhang and Y. Chen, *Carbon*, 2013, 63, 508-516.
 70. J. Shen, Y. Hu, M. Shi, X. Lu, C. Qin, C. Li and M. Ye, *Chemistry of Materials*, 2009, 21, 3514-3520.

List of figures:

Figure 1. Schematic diagram for the synthesis of the ternary GMP composite.

Figure 2. XRD patterns of pure graphene oxide, MoO₃, PpPD and ternary GMP-1.0 composites.

Figure 3. Raman spectra collected for pure graphene oxide, MoO₃, PpPD and ternary GMP-1.0 composites, respectively.

Figure 4. FT-IR patterns of pure graphene oxide, MoO₃, PpPD and ternary GMP-1.0 composites.

Figure 5. Wide scan XPS spectrum (a); Mo 3d (b), and N1s (c) of ternary GMP-1.0 composites; C1s spectra of GO (d) and ternary GMP-1.0(e).

Figure 6. TEM images of GO (a) and ternary GMP-1.0 composites (b); FESEM images of pure MoO₃(c), PpPD (d) and ternary GMP-1.0 (e).

Figure 7. CV curves of pure reduced graphene, MoO₃ and PpPD at 5 mV s⁻¹(a); CV curves of binary GP, GM, MP and ternary GMP-1.0 composites at 5 mV s⁻¹(b); CV curves of ternary GMP-1.0 composites at differing scan rates in 1 M H₂SO₄ (c).

Figure 8. GCD curves of binary GP, GM, MP and ternary GMP-1.0 composites at current density of 1 A g⁻¹ (a); GCD curves of ternary GMP-1.0 composites at different current densities (b); AC impedance spectra of binary GP, GM, MP and ternary GMP-1.0 composites (c); and variation of capacitance retention loss of ternary GMP-1.0 at current density of 12 A g⁻¹ in 1 M H₂SO₄ (d) and inset is corresponding GCDs curves.

Figure 9. CV curves of GMP-1.0//GMP-1.0 devices in the 1 M H₂SO₄ solutions

at different scan rates (a); GCD curves of GMP-1.0//GMP-1.0 devices at different current densities (b); Ragone plot for GMP-1.0//GMP-1.0 devices (c).

Figure 1

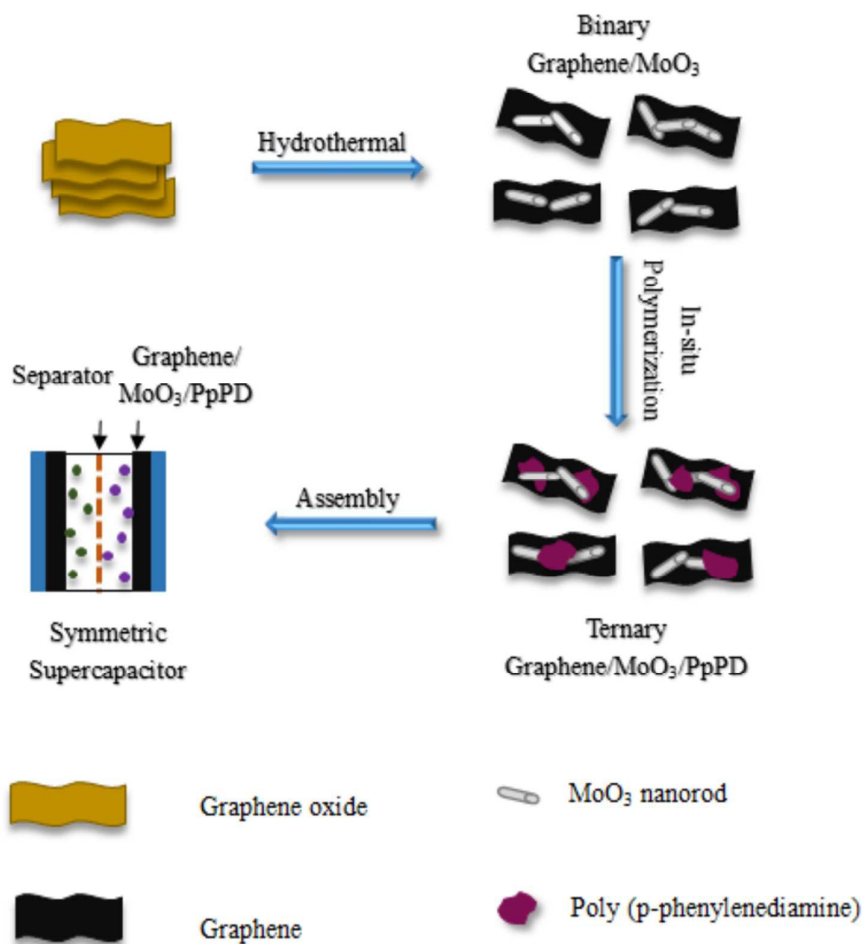


Figure 2

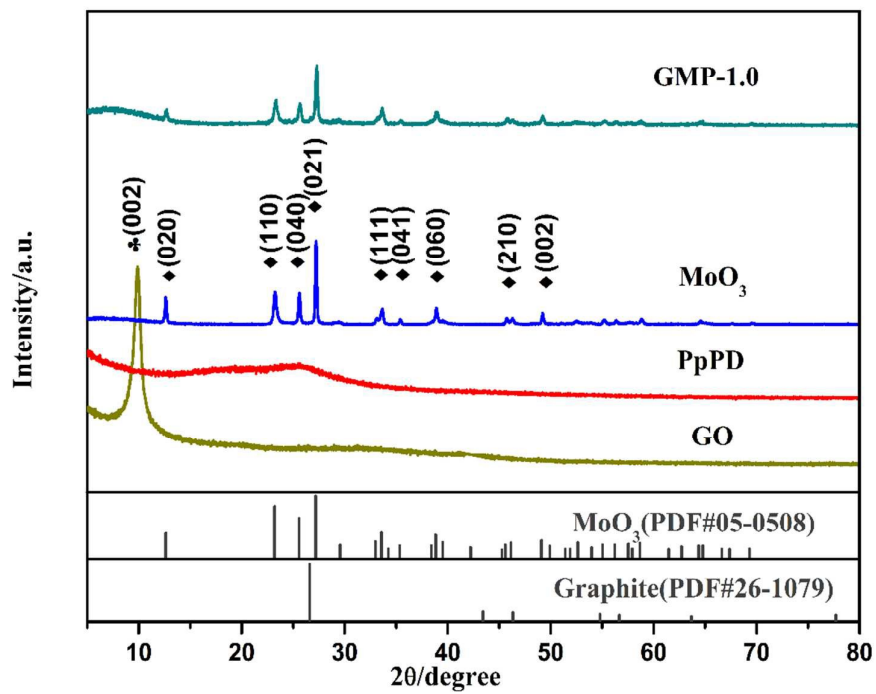


Figure 3

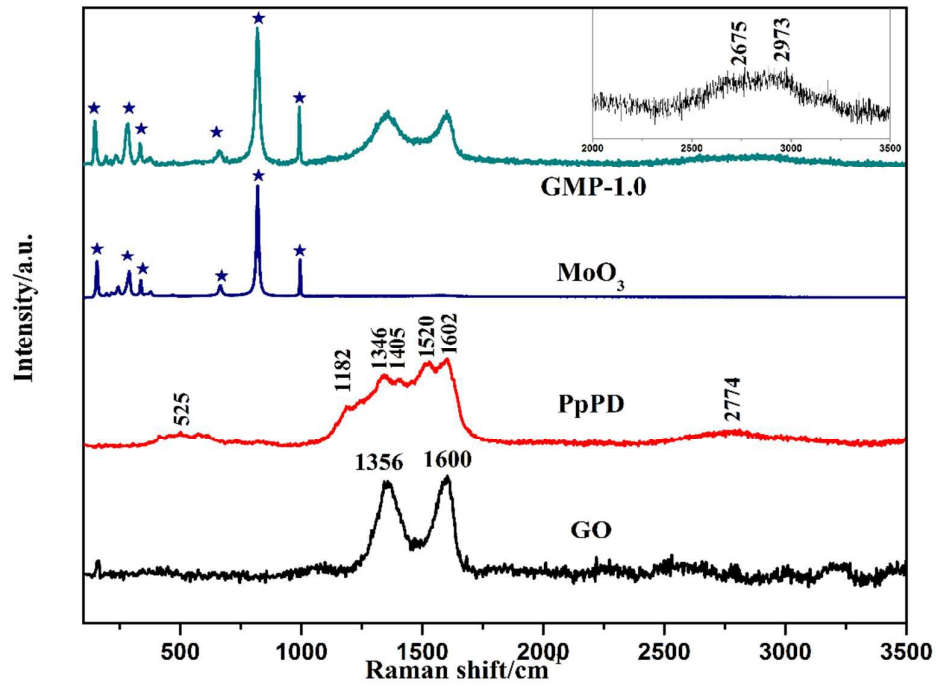


Figure 4

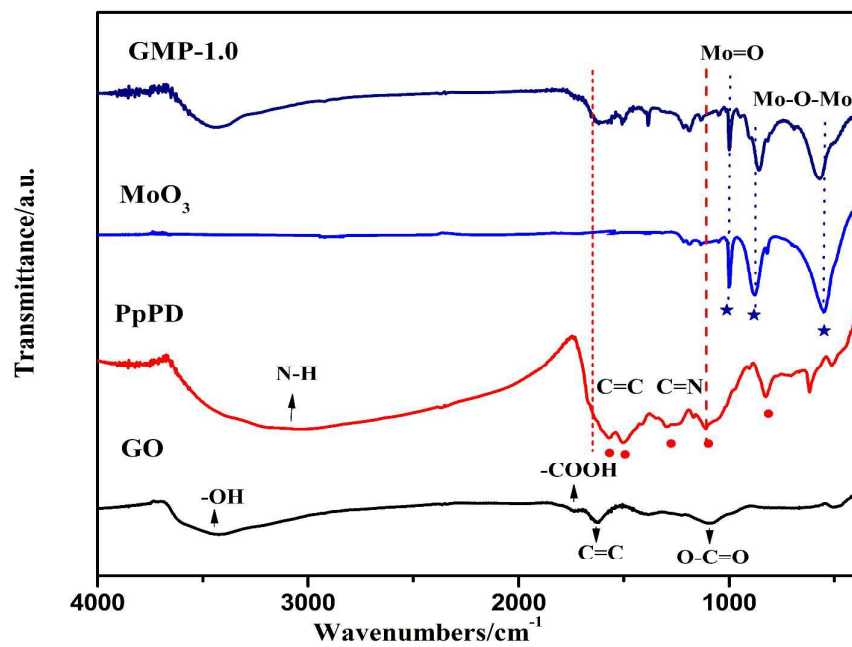


Figure 5

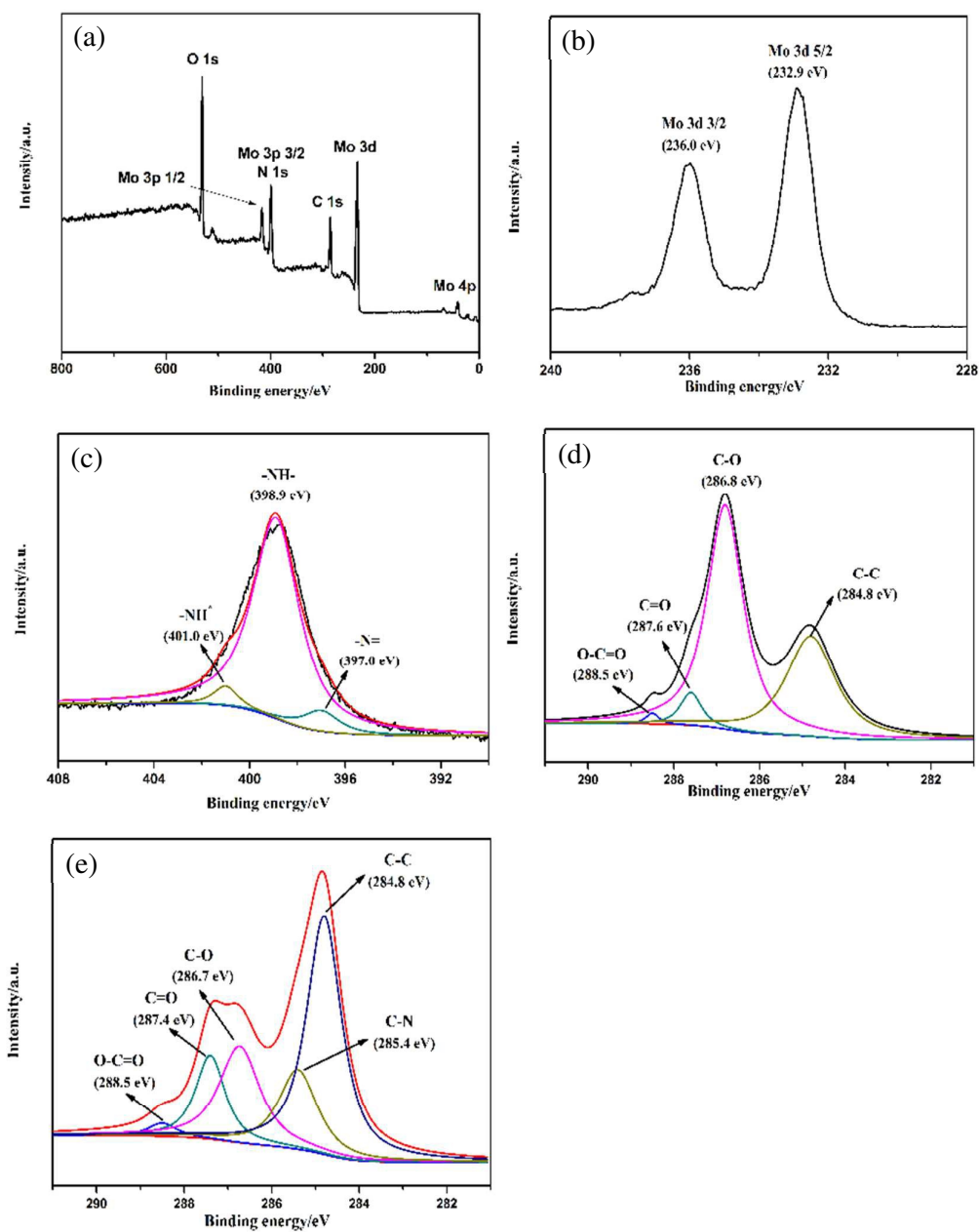


Figure 6

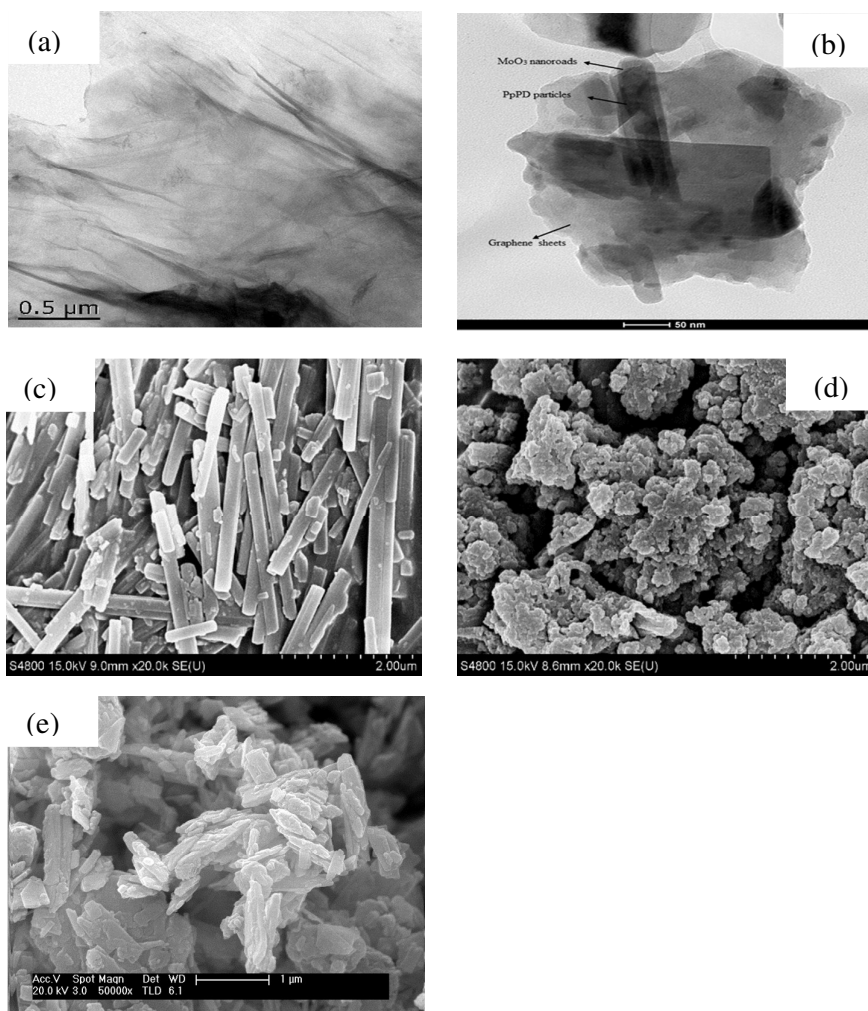


Figure 7

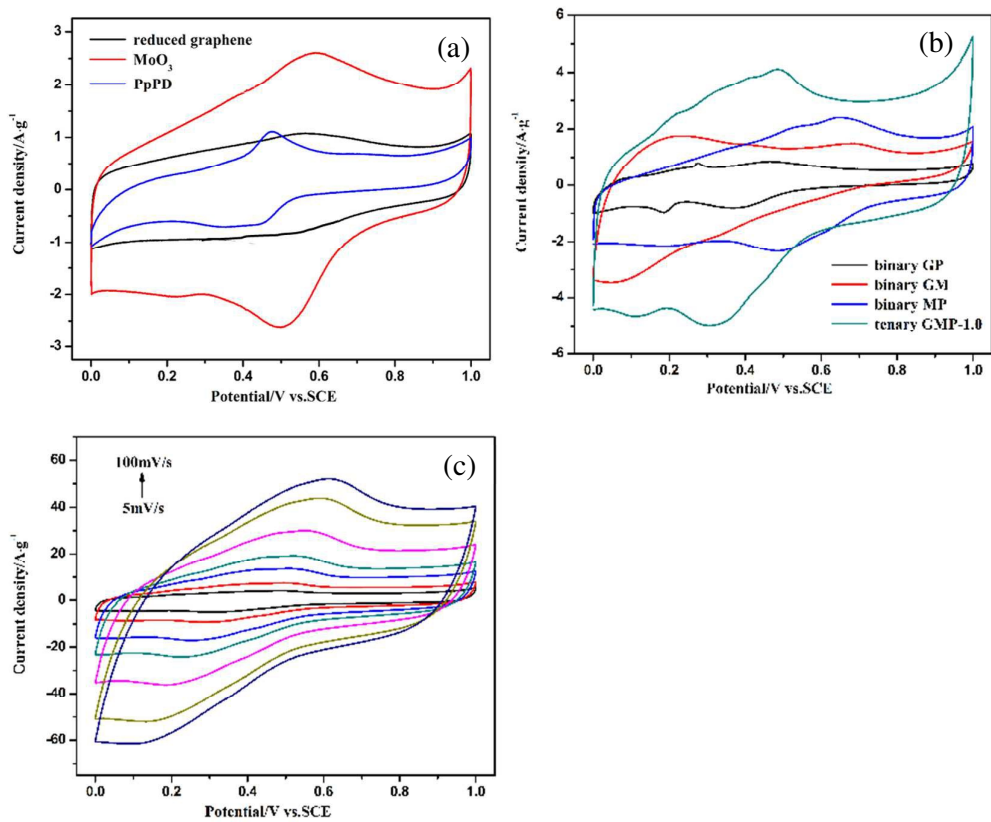


Figure 8

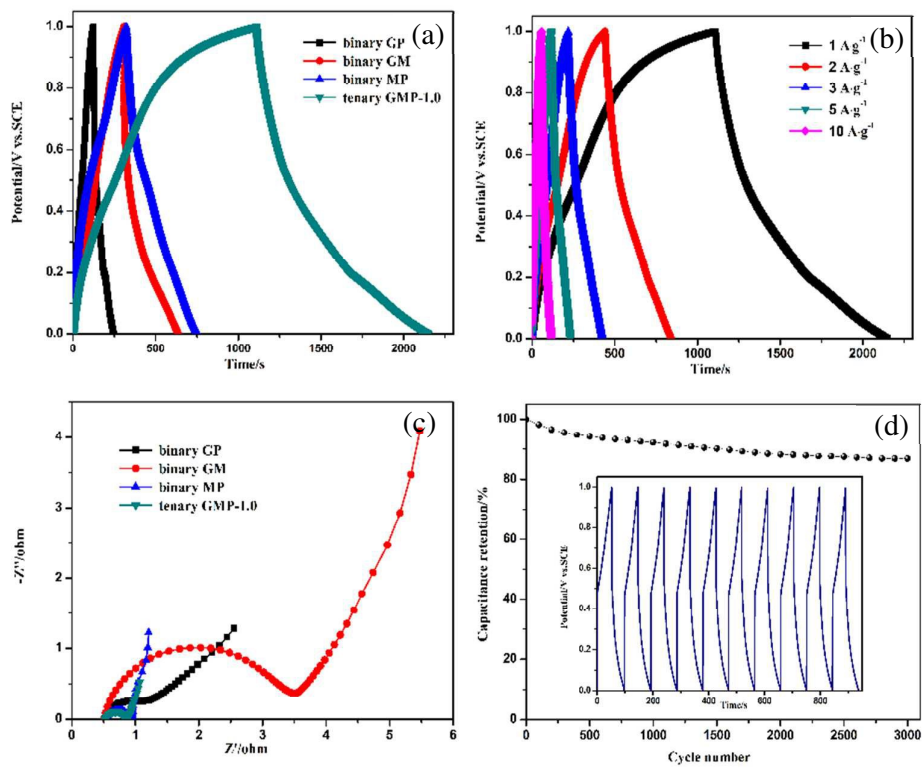


Figure 9

